UC Riverside
UC Riverside Previously Published Works

Title

Inflammatory response to implantation of transparent nanocrystalline yttria-stabilized zirconia using a dorsal window chamber model

Permalink

Journal

ISSN

Authors

Damestani, Yasaman
Galan-Hoffman, Diego E
Ortiz, Daniel
et al.

Publication Date

DOI

Peer reviewed

Inflammatory response to implantation of transparent nanocrystalline yttria-stabilized zirconia using a dorsal window chamber model

Yasaman Damestani, PhD[a], Diego E. Galan-Hoffman, BS[b], Daniel Ortiz, MS[b],
Pedro Cabrales, PhD[b], Guillermo Aguilar, PhD[c],*

[a]Department of Bioengineering, University of California Riverside, Riverside, CA, USA
[b]Department of Bioengineering, University of California San Diego, La Jolla, CA, USA
[c]Department of Mechanical Engineering, University of California Riverside, Riverside, CA, USA

Abstract

The long-range goal of the windows to the brain (WttB) is to improve patient care by providing a technique for delivery and/or collection of light into/from the brain, on demand, over large areas, and on a chronically-recurring basis without the need for repeated craniotomies. To evaluate the potential of nanocrystalline yttria-stabilized-zirconia (nc-YSZ) cranial implant for optical therapy and imaging, in vivo biocompatibility was studied using the dorsal window chamber model in comparison with control (no implant) and commercially available cranial implant materials (PEEK and PEKK). The host tissue response to implant was characterized by using transillumination and fluorescent microscopy to measure leukocyte adhesion, blood vessel diameter, blood flow rate, and vascular permeability over two weeks. The results indicated the lack of inflammatory reaction of the host tissue to nc-YSZ at the microscopic level, suggesting that nc-YSZ is a good alternative material for cranial implants.

Craniotomy is an established procedure in neurosurgery to decrease intracranial pressure after brain infarction, intracranial hemorrhage, and brain traumatic injury resulting from cerebral edema. During this procedure parts of the brain become exposed, leaving it unprotected and giving the patient a malformed appearance. Cranioplasty is the subsequent surgical procedure to restore the aesthetic appearance of the cranium and provide the necessary mechanical protection to the brain. A successful cranioplasty has shown to improve electroencephalographic abnormalities, cerebral blood flow abnormalities, and other neurological abnormalities.[1-3] The ideal material used for cranioplasty needs to be 1) radiolucent, 2) resistant to infections, 3) thermal insulator, 4) resistant to mechanical load, 5) malleable to fit defects with complete closure, and ideally, 6) inexpensive.[4] Over time, a broad spectrum of synthetic materials has been used for cranioplasty,[5] including titanium and PEEK (poly-ether-ether ketone).[6,7] A new thermoplastic matrix system PEKK (poly-ether-ketone-ketone), resembles bone more so than titanium.[8,9] PEEK and PEKK are more elastic and are less dense which pose some advantages, whereas titanium has a higher yield and ultimate strength, making it mechanically more stable.[10] PEKK has higher compressive strength than PEEK and has demonstrated to have superior performance in mechanical properties, fracture toughness and damage tolerance.[11,12]

All these materials seem appropriate to protect the brain against mechanical trauma. However, these polymers do not provide the requisite combination of properties required for clinically-viable transparent implants. During the past few years, researchers have been working on several promising options to circumvent the limitations of current materials for cranial reconstruction.[5] Our group has aimed to develop a novel transparent ceramic material capable of providing access to the brain for imaging and therapeutic purposes.[13] This material is nanocrystalline yttria-stabilized-zirconia (nc-YSZ), and it is synthesized by a relatively new densification process known as current activated pressure assisted densification (CAPAD) technique.[14,15] YSZ produced using conventional ceramic processing methods is typically opaque, due to scattering induced by micrometer-scale (and larger) internal porosity.[16]

*Corresponding author at: Department of Mechanical Engineering, University of California Riverside, Riverside, CA, USA.

CAPAD technique enables reduction of internal porosity to nanometric dimensions. At this length scale, porosity is sufficiently small to minimize scattering in the spectral range of interest for laser-based diagnostics and therapeutics.[16]

Nc-YSZ implants will provide a combination of transparency, toughness, and biocompatibility to support angiogenesis, and neovascularization, for clinically-viable transparent cranial implants.[10,17] The dorsal window chamber model (DWCM) is widely used to chronically study the intact microcirculation.[18] DWCM allows for the in vivo analysis of biocompatibility, as it allows long-term quantification of hemodynamic, angiogenic, and inflammatory response for several weeks after material implantation.[19] DWCM has been previously used to study the biocompatibility of ceramic, and titanium.[20-22]

The objective of the study is to quantify hemodynamic and inflammatory changes resulting from implantation of nc-YSZ, PEEK, and PEKK in the DWCM. The study tests the hypothesis that the biocompatibility of nc-YSZ is superior to currently used material for cranioplasty, PEEK and PEKK. Biocompatibility is assessed in our study in terms of hemodynamics, vascular permeability, and leukocyte activation.

Materials and methods

Animal model and implantation

Animal handling and care were provided following the Care and Use of Laboratory Animals.[23] All animal experiments were conducted under a protocol approved by the University of California, San Diego Institutional Animal Care and Use Committee (S04052, Microhemodynamics of Hamster Skinfold Model, approved on 04/04/2015). Male golden Syrian hamsters of 50-70 g were fitted with a one-sided window chamber consisting of two titanium supports, one of which holds a 12-mm-diameter glass window. The complete surgical technique was reported previously.[24,25] Briefly, the animals were prepared for chamber implantation with a long acting anesthetic, sodium pentobarbital (i.p. 50 mg/kg).[24] After hair removal, two sutures were used to lift the dorsal skin of the back away from the animal and one frame of the chamber was positioned on the animal's back. With the aid of backlighting and a stereomicroscope, following the outline of the window, skin was removed until only a thin monolayer of retractor muscle and the intact subcutaneous skin of the opposing side remained.

Implantation

A small square of 2 by 2 mm with a thickness of 100 μm was cut and sterilized prior to implantation. Nc-YSZ (fabricated by CAPAD technique),[15] PEEK (McMaster-Carr, Los Angeles, CA), and PEKK (Oxford Performance Materials, South Windsor, CT) were placed directly onto the striated muscle and subcutaneous tissue under the cover slip (Figure 1). During implantation, a drop of saline solution was used to hold the sample in place between the exposed skin and the frame of the chamber. Stainless steel nuts between the frames were used as spacers (450 to 500 μm). The animal was allowed to rest for 2 days, at which time its chamber was evaluated under the microscope (650×) for any sign of infection, edema, or bleeding. Animals absent of any microvascular complication were anesthetized again with sodium pentobarbital and arterial and venous catheters (PE-50) in the carotid artery and jugular vein were implanted, respectively. Catheters were filled with heparinized saline (40 IU/ml), to ensure patency. Catheters were tunneled under the skin and exteriorized at the dorsal side of the neck where they were attached to the chamber frame.

Inclusion criteria

Hamsters were suitable for the experiments if: 1) systemic parameters were within normal range. Namely, heart rate (HR) >350 beat/min, mean arterial blood pressure (MAP) >80 mmHg, systemic hematocrit (Hct) >45%, arterial PO_2 pressure (PaO_2) >50 mmHg and arterial PCO_2 pressure ($PaCO_2$) >35 mmHg; and 2) microscopic examination of the tissue in the chamber observed under ×650 magnification did not reveal signs of edema or bleeding. Hamsters are fossorial animals with a low arterial PO_2 compared to other rodents; however, the PO_2s in the window chamber are similar to the PO_2s in other rodents.[26]

Experimental groups

Animals were assigned randomly to the different experimental groups. Groups are labeled based on the material implanted. A prior calculation of the sample size to evaluate changes in blood flow after implantation in DWCM, suggested that blood flow after one week implantation of nc-YSZ, presented a standard deviation of 17% and expected difference from baseline of 130% (mean: 2.3 relative to baseline, and SD = 0.4 relative to baseline). Therefore, the minimal number of experiments using a power analysis with alpha of 0.05 and a 1-beta of 0.9 estimated 4 animals were required to detect changes in blood flow from baseline. Accordingly, the study includes four animals experimental group: 1) Control ($n = 4$, without any implant); 2) nc-YSZ ($n = 7$); PEEK ($n = 4$); and PEKK ($n = 4$). The additional animals in nc-YSZ were used to develop the model.

Intravital microscopy experimental setup

The animals were restrained in a Plexiglas tube, which allows the window chamber to protrude and be fixed to the microscope stage. Observations were completed using transillumination (BX51WI, Olympus, New Hyde Park, NY).

Measurements were carried out using a 40X (LUMPFL-WIR, NA 0.8, Olympus) water immersion objective. Animals were given 10 to 15 min to adjust to the tube environment before any measurement. Detailed mappings were made of the chamber vasculature to follow the same vessels studied at baseline throughout the experiment. Blood vessels were chosen by a distinctive anatomic landmark. Tissue was illuminated with a mercury arc lamp (100 W, Walker Instruments, Scottsdale, AZ) and a 400 nm filter (Spectra Physics, no. 59820). Images were recorded with a high speed video camera (1000 × 1000 pixels, 2000 fps, Fastcam 1024 PCI, Photron, San Diego, USA). Camera shutter speed was 1/10 of the frame rate.

Microhemodynamics

A video image-shearing method was used to measure vessel diameter (D).[27] This technique possesses a resolution of 1 μm for vessels of 15-20 μm diameter and greater, and it measures the
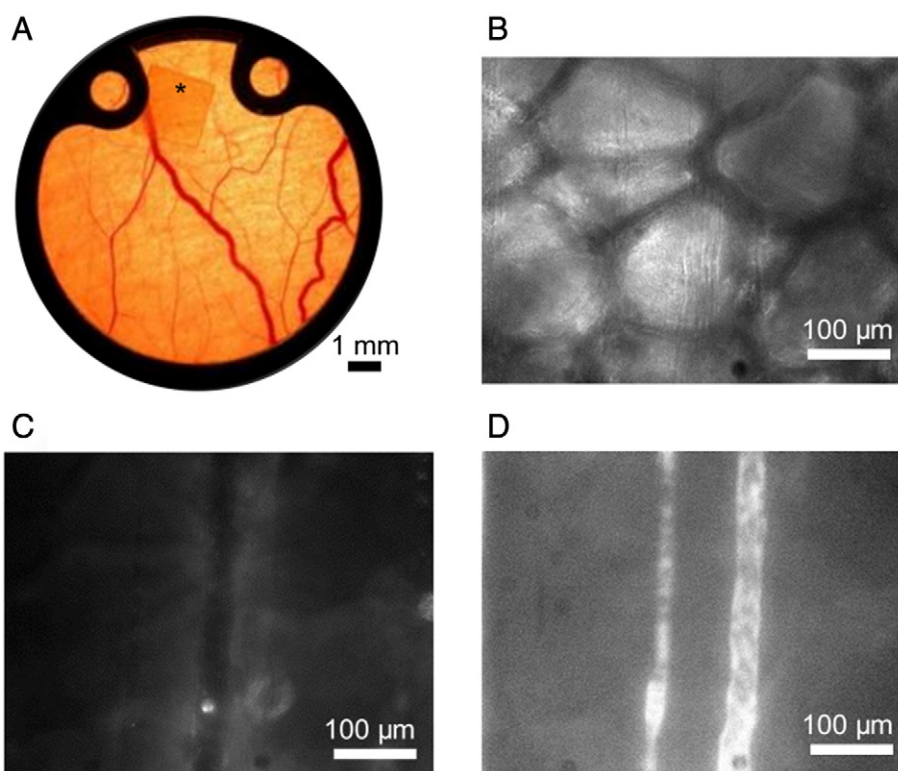
Figure 1. (**A**) Photograph of dorsal skinfold chamber of Syrian golden hamsters, containing striated muscle and skin and allowing for repeated analysis of the microcirculation in an awaken hamster for two weeks. Here a nc-YSZ sample (*) was implanted. (**B, C, D**) Representative intravital fluorescence microscopy image of the microcirculation under the nc-YSZ implant 15 days after implantation at 20× with: (**B**) white light; (**C**) green-light epi-illumination upon injection of Rhodamine 6G for direct labeling of activated leukocytes. (**D**) Blue-light epi-illumination upon injection of macromolecular fluorescent dye FITC-labeled Dextran.

diameter on-line without the need to digitize and post process image files. Image sheering device is not subjective, as it is based on the distance in pixels between edges of blood vessels.[27] Changes in arteriolar and venular diameter from baseline were used as indicators of a change in vascular tone. Arteriolar and venular centerline velocities were measured off-line using the image cross-correlation method.[28] This method was selected over laser Doppler velocimetry as it allows for blood flow measurements of specific blood vessels near the implanted materials. The measured centerline velocity (V) was corrected according to vessel size to obtain the mean RBC velocity.[29] Blood flow (Q) was calculated from the measured values as $Q = \pi \times V (D/2)$.[2]

Leukocyte endothelial interaction

To label leukocytes, animals received intravenous injection of 5 mg/kg of Rhodamine 6G (Sigma-Aldrich, St Louis) infused in a volume equal to 0.1 mL. Fluorescently labeled leukocytes were excited and images were captured with a Vivid Set (XF104-2 filter, Omega Filters, Brattleboro, VT) using a low light camera (ORCA 9247, Hamamatsu, Tokyo, Japan). Briefly, a straight portion of blood vessels was illuminated for 60 sec and video was recorded (10 frames/s). Leukocytes were counted during video playback in a 100 μm length segment and categorized according to their flow behaviour as "free-flowing", "rolling" on the endothelium, and

"immobilized" cells.[30] The rolling leukocytes were white cells rolling on the endothelium and reported as the percentage of all leukocytes passing, "free-flowing".

Macromolecule vascular permeability

Vascular permeability was studied after infusion in a volume equal to 0.1 mL of an intravenous injection of 5 mg/kg fluorescein isothiocyanate (FITC)-conjugated dextran with a molecular weight of 150 kDa (FITC-dextran). Fluorescent macromolecular permeability was studied by measuring the fluorescence intensities of the perivascular and intravascular space for the blood vessels studied. FITC-dextran fluorescence were excited and images were captured with a Vivid Set (XF25 filter, Omega Filters, Brattleboro, VT) using a low light camera (ORCA 9247, Hamamatsu, Tokyo, Japan). Fluorescence levels were measured using ImageJ (Java-based image processing program developed at the NIH by Wayne Rasband, http://rsb.info.nih.gov/ij/). Intensities of the perivascular space directly adjacent to the blood vessel wall (E_1) and intensity of the intravascular space (E_2), were used to estimate an extravasation index (E), defined as $E = E_1/E_2$.

Microvascular experimental protocol

Awaken animals were restrained in a Plexiglas tube from which the window chamber protrudes and the restraining tube was fixed to the intravital microscope stage. Hemodynamic measurements
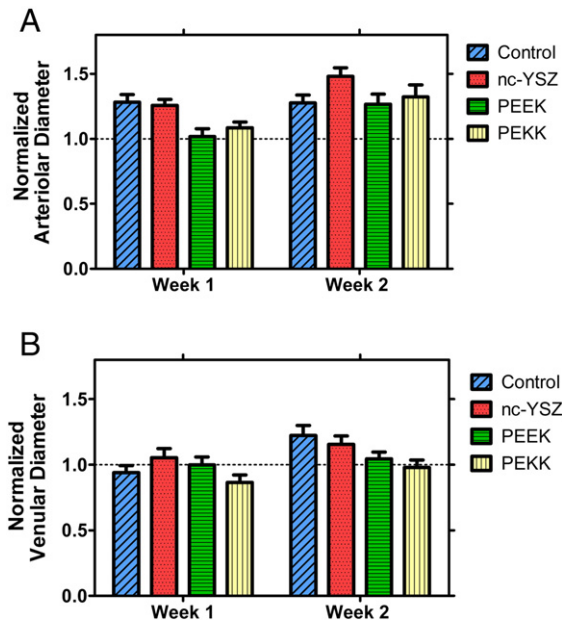
Figure 2. Normalized arteriolar (**A**) and venular (**B**) diameter of dorsal skinfold chamber of hamsters implanted with nc-YSZ, PEEK and PEKK in comparison with control (no implant).

Figure 3. Normalized arteriolar (**A**) and venular (**B**) velocity of dorsal skinfold chamber of hamsters implanted with nc-YSZ, PEEK and PEKK in comparison with control (no implant). 2-way ANOVA repeated measures, Bonferroni post-test *$P < 0.05$ relative to control.

were made 2, 5, 7, 10, 12 and 15 days after material implantation. Leukocyte endothelia interaction and macromolecule vascular permeability were studied 15 days after material implantation. Microhemodynamics, leukocyte-endothelial interaction, and macromolecule permeability were assessed in different microvascular regions of interest (ROI) including tissue behind the implant, tissue surrounding the implant, and tissue far away from the implant. In each ROI, six to eight arterioles and venules were selected in each preparation. Fields of observation and vessels were chosen for study at locations in the tissue where the vessels were in sharp focus. After 15 days, animals were euthanized.

Statistical analysis

Results are presented as mean ± standard error of the mean (SEM). Hemodynamic results within each group were analyzed using analysis of variance for repeated measurements (ANOVA, Kruskal-Wallis test). When appropriate, post hoc analyses were performed with the Dunn's multiple comparison test. Hemodynamic data comparison between groups was analyzed using two-way analysis of variance (two-way ANOVA test). When appropriate, post-test analyses were performed with the Bonferroni post-tests comparison. Leukocytes adherent and rolling, and vascular permeability of each groups were tested for normality according to the Shapiro-Wilk test, and analyzed using analysis of variance for repeated measurements (ANOVA, Brown-Forsythe test). When appropriate, post hoc analyses were performed with the Bonferroni's multiple comparisons test. Microhemodynamic data is presented normalized to day 2 after implantation. All statistics were calculated using GraphPad Prism 5.01 (GraphPad Software, Inc., San Diego, CA). Changes were considered statistically significant if $P < 0.05$.
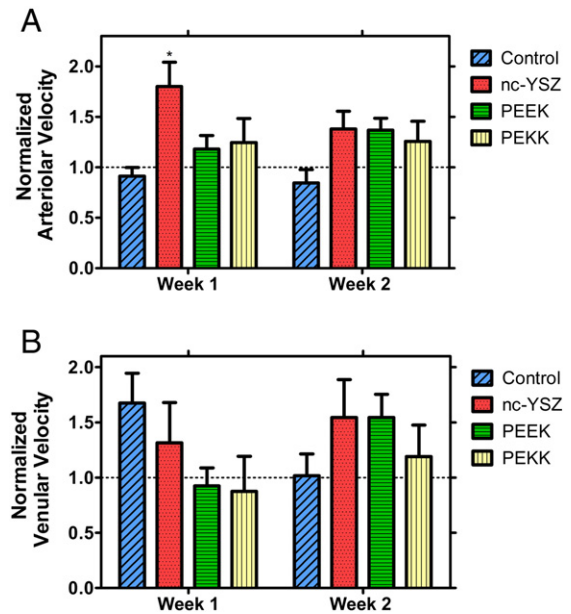
Results

All animals completed the study protocol without visible sign of discomfort. Animals were observed resting and periodically eating throughout the experiment. In Figures 2-4, week 1 consisted of data collected on days 5 and 7, and week 2 consisted of data collected on days 10, 12, and 15.

Microhemodynamics: Microvascular diameter

Diameter of a total number of 45 arterioles was investigated (control, $n = 8$; nc-YSZ, $n = 20$, PEEK, $n = 8$, PEKK, $n = 9$, where n corresponds to the number of microvessels study per group). Range of inner diameter of baseline arterioles proved to be similar in all groups (control, 34-68 μm; nc-YSZ, 36-84 μm; PEEK, 39-68 μm; PEKK, 24-70 μm). No statistically significant difference was observed in microvascular variables measured at day 2 between groups. The results in Figure 2, *A* indicated that the mean arterioles in animals in all four groups exhibited slight vasodilation over two weeks (mean >1). However, the vasodilation was not statistically significant for implants in comparison with control in each week.

Diameter of a total number of 52 venules was investigated (control, $n = 12$; nc-YSZ, $n = 21$; PEEK, $n = 10$; PEKK, $n = 9$). Range of baseline venules was similar in all groups (control, 28-68 μm; nc-YSZ, 27-84 μm; PEEK, 32-68 μm; PEKK, 35-70 μm). The results in Figure 2, *B* reveal almost constant venular diameters over time, with minor difference between groups.

Microhemodynamics: Microvascular velocity

The computed velocity profiles characterized by the velocity of RBC and obtained from in vivo videos depict a parabolic
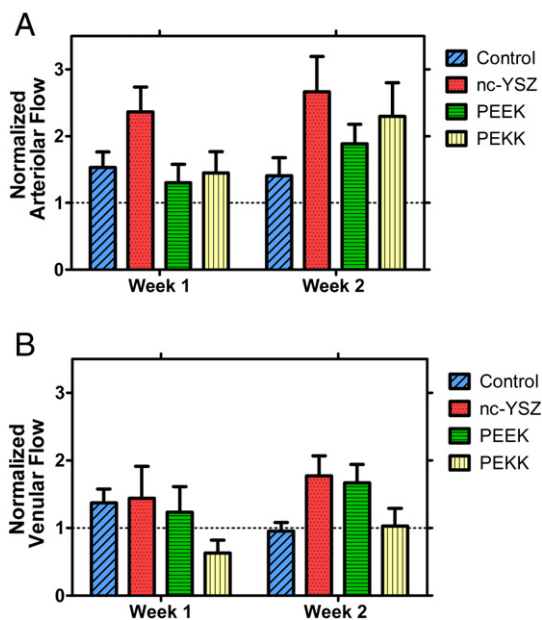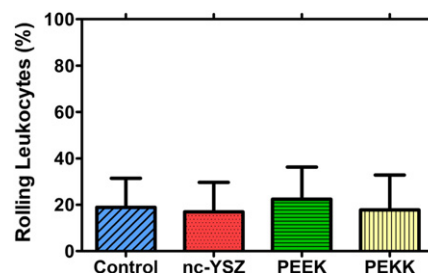
Figure 5. Number of rolling leukocytes (given in % of non-adherent leukocytes) in venules of hamster dorsal skinfold 15 days after control (no implant) and implantation of nc-YSZ, PEEK, PEKK. $N = 20$ for each condition and error bars represent 1 standard deviation.

Figure 4. Normalized arteriolar (**A**) and venular (**B**) flow of dorsal skinfold chamber of hamsters implanted with nc-YSZ, PEEK and PEKK in comparison with control (no implant).

shape based on a Newtonian fluid laminar flow assumption. Velocity of a total of 39 arterioles was investigated for two weeks (control, $n = 20$; nc-YSZ, $n = 7$; PEEK, $n = 6$; PEKK, $n = 6$). Range of baseline arteriolar velocity was similar in all groups (control, 0.31-3.95 mm/s; nc-YSZ, 1.58-5.12 mm/s; PEEK, 0.96-2.65 mm/s; PEKK, 0.72-3.29 mm/s). Figure 3, *A* shows that the implantation of nc-YSZ seems to initially evoke a statistically significant increase in arteriolar velocity in comparison with control. However, the arteriolar velocity declined in the second week and reached a value comparable to control, PEEK, and PEKK.

Velocity of a total of 46 venules was investigated for two weeks (control, $n = 15$; nc-YSZ, $n = 14$; PEEK, $n = 7$; PEKK, $n = 10$). Range of baseline venular velocity was similar in all groups (control, 0.49-5.04 mm/s; nc-YSZ, 0.31-4.21 mm/s; PEEK, 0.12-3.51 mm/s; PEKK, 0.12-0.72 mm/s). Figure 3, *B* shows that during the first week, the venular velocity for animals with PEEK and PEKK was decreased while it increased for control and nc-YSZ. However, the difference in the venular velocity of all groups during two weeks was not statistically significant.

Microhemodynamics: Microvascular flow

Figure 4 reveals that the changes in arteriolar and venular flow in animals of all groups were not statistical significant. The slight increase in arteriolar flow over time is due to anatomical changes and vasodilation over two weeks. Therefore, data indicated that the microvascular blood flow of animals was not impaired by implantation of the materials.

Inflammation: Leukocyte-endothelial cell interaction

In each group, 30 venules were analyzed after two weeks. Figure 5 demonstrated that nc-YSZ only induced a transient change

in leukocyte endothelial cell interactions in venules of the host tissue (17%) in comparison with the control (19%) after the first 15 days of implantation, indicating a high degree of biocompatibility. The lack of an inflammatory reaction to implants (no statistical significance) indicated an adequate biocompatibility of nc-YSZ, comparable to that of PEEK, PEKK and control hamsters.

Microvascular permeability

The macromolecular leakage was increased for all implant groups with no statistical significance (Figure 6). For all groups, the macromolecular leakage values were below 0.8-1, an intact endothelial integrity can be assumed.[31] Therefore, nc-YSZ did not increase vascular permeability when compared to control and commercial implants.

Discussion

In this report, the DWCM was used to study the microcirculation by means of intravital microscopy using transillumination. Previously, this model proved to be ideal for the systematic in vivo analysis of the host tissue interaction with biomaterials.[18,19,32] Specifically, this model has been used to study the host tissue response to cranioplasty biomaterials such as ceramic calcium phosphate compounds[20,21] and titanium.[22,32,33]

Conventionally-processed microcrystalline YSZ (mc-YSZ) has well-proven biocompatibility in dental and orthopedic applications.[17] However, biocompatibility assessments for nc-YSZ specifically are necessitated by the unique properties associated with nanocrystallinity (e.g. increased surface energy). The prolonged inflammatory response to an implant is one of the primary causes for the failure to integrate into tissue.[5]

Figure 2 demonstrated that changes in arteriolar and venular diameter in hamsters with nc-YSZ implant were not significantly different than those of control and commercially available implants (PEEK and PEKK). Significant vasodilation in the DWCM would be an initial sign of infection or acute inflammation.[18] Figure 3 revealed a statistically significant increase in the arteriolar velocity of hamsters with nc-YSZ implants in comparison with control in week 1. However, by week 2, this difference decreased and became insignificant. Figure 4 shows insignificant difference between the microvascular blood flow of all groups, indicating that implants did not disturb the blood flow.
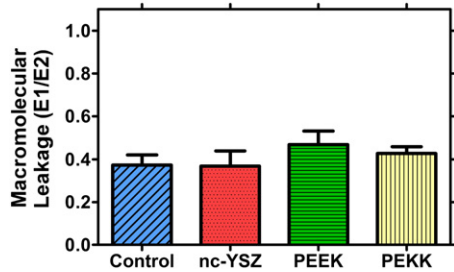
Figure 6. Macromolecule leakage as an indicator of microvascular permeability in venules of striated muscle in hamster dorsal skinfold 15 days after control (no implant) and implantation of nc-YSZ, PEEK, PEKK. $N = 20$ for each condition and error bars represent 1 standard deviation.

Analysis of microvascular permeability by quantifying the extravasation of macromolecules, shown in Figure 6, indicated that the endothelial lining of postcapillary and collecting venules were not damaged as a result of nc-YSZ implantation. Additionally, we have demonstrated the lack of activated leukocytes in venules for all groups, indicating that the nc-YSZ, PEEK, and PEKK did not induce an acute inflammatory response in the host tissue. Thus, nc-YSZ exhibited a good biocompatibility that was comparable to that of control, PEEK and PEKK.

While PEEK and PEKK are FDA-approved commercially available cranial implants, this is the first study, to the best of our knowledge, to observe microhemodynamics changes in a hamster backflap model in response to PEEK and PEKK implants. One limitation of using the DWCM to study biomaterial reaction is that this model cannot directly predict the bone ingrowth and response around the implant. Comprehensive characterization of nc-YSZ as a cranial material should be performed by combining the results of this study with other models such as calvarial defect model.[34] Future studies with nc-YSZ will include dynamic stimulus (e.g. change in pCO_2) to understand the effects of nc-YSZ cranial implants on cerebral blood flow regulation.

In summary, this study demonstrated that nc-YSZ does not impair microcirculation and endothelial integrity of striated muscle in the DWCM. The nc-YSZ also did not result in enhanced leukocyte activation and was as equally tissue-compatible as commercial PEEK and PEKK cranioplasty materials. Clinically, the results presented in this report indicate that nc-YSZ may represent a good alternative for cranial implants.

Acknowledgments

References

1. Chun H-J, Yi H-J. Efficacy and safety of early cranioplasty, at least within 1 month. *J Craniofac Surg* 2011;**22**:203-7.
2. Winkler PA, Stummer W, Linke R, Krishnan KG, Tatsch K. Influence of cranioplasty on postural blood flow regulation, cerebrovascular reserve capacity, and cerebral glucose metabolism. *J Neurosurg* 2000;**93**:53-61.
3. Chiarini L, Figurelli S, Pollastri G, Torcia E, Ferrari F, Albanese M, et al. Cranioplasty using acrylic material: a new technical procedure. *Surg* 2004;**32**:5-9.
4. Rodríguez B, Romero A, Soto O, de Varorna O. *Biomaterials for orthopedics*. Applications of Engineering Mechanics in Medicine; 20041-26.
5. Cho YR, Gosain AK. Biomaterials in craniofacial reconstruction. *Clin Plast Surg* 2004;**31**:377-85 [v].
6. Camarini ET, Tomeh JK, Dias RR, da Silva EJ. Reconstruction of frontal bone using specific implant polyether-ether-ketone. *J Craniofac Surg* 2011;**22**:2205-7.
7. Heissler E, Fischer FS, Bolouri S, Lehmann T, Mathar W, Gebhardt A, et al. Custom-made cast titanium implants produced with CAD/CAM for the reconstruction of cranium defects. *Oral Maxillofac Surg* 1998;**27**:334-8.
8. Katzer A, Marquardt H, Westendorf J, Wening JV, von Foerster G. Polyetheretherketone – cytotoxicity and mutagenicity in vitro. *Biomaterials* 2002;**23**:1749-59.
9. Eschbach L. Nonresorbable polymers in bone surgery. *Injury* 2000;**31**(Suppl 4):22-7.
10. Wong KL, Wong CT, Liu WC, Pan HB, Fong MK, Lam WM, et al. Mechanical properties and in vitro response of strontium-containing hydroxyapatite/polyetheretherketone composites. *Biomaterials* 2009;**30**:3810-7.
11. Chang IY. PEKK as a new thermoplastic matrix for high-performance composites. *Sampe Quart* 1988;**19**:29-34.
12. Chang IY, Lees JK. Recent development in thermoplastic composites: A review of matrix systems and processing methods. *J Thermoplast Compos Mater* 1988;**1**:277-96.
13. Damestani Y, Reynolds CL, Szu J, Hsu MS, Kodera Y, Binder DK, et al. Transparent nanocrystalline yttria-stabilized-zirconia calvarium prosthesis. *Nanomedicine* 2013;**9**:1135-8.
14. Garay JE. Current-activated, pressure-assisted densification of materials. *Annu Rev Mater Res* 2010;**40**:445-68.
15. Kodera Y, Hardin CL, Garay JE. Transmitting, emitting and controlling light: Processing of transparent ceramics using current-activated pressure-assisted densification. *Scr Mater* 2013;**69**:149-54.
16. Alaniz JE, Perez-Gutierrez FG, Aguilar G, Garay JE. Optical properties of transparent nanocrystalline yttria stabilized zirconia. *Opt Mater* 2009;**32**:62-8.
17. Christel P, Meunier A, Heller M, Torre JP, Peille CN. Mechanical properties and short-term in-vivo evaluation of yttrium-oxide-partially-stabilized zirconia. *J Biomed Mater Res* 1989;**23**:45-61.
18. Laschke M, Vollmar B, Menger M. The dorsal skinfold chamber: Window into the dynamic interaction of biomaterials with their surrounding host tissue. *Eur Cell Mater* 2011;**22**:147-64.
19. Menger MD, Laschke MW, Vollmar B. Viewing the microcirculation through the window: Some twenty years experience with the hamster dorsal skinfold chamber. *Eur Surg Res* 2002;**34**:83-91.
20. Roetman B, Ring A, Langer S, Schildhauer TA, Muhr G, Koller M. Microvascular response to calcium phosphate bone substitutes: An intravital microscopy analysis. *Langenbecks Arch Surg* 2010;**395**:1147-55.
21. Kraft CN, Weber W, Burian B, Zander D, Wallny T, Schmitt O, et al. Striated muscle microvascular response to implants with sol–gel calcium phosphate coating. A comparative in vivo study. *Z Orthop Ihre Grenzgeb* 2002;**140**:672-80.
22. Pennekamp PH, Gessmann J, Diedrich O, Burian B, Wimmer MA, Frauchiger VM, et al. Short-term microvascular response of striated muscle to cp-Ti, Ti-6Al-4 V, and Ti-6Al-7Nb. *J Orthop Res* 2006;**24**:531-40.
23. Institute of Laboratory Animal Resources (U.S.). Committee on Care and Use of Laboratory Animals. *Guide for the care and use of laboratory animals*. Washington, D.C.: National Academies Press; 2011.

24. Endrich B, Asaishi K, Gotz A, Messmer K. Technical report – a new chamber technique for microvascular studies in unanesthetized hamsters. *Res Exp Med (Berl)* 1980;**177**:125-34.

25. Colantuoni A, Bertuglia S, Intaglietta M. Quantitation of rhythmic diameter changes in arterial microcirculation. *Phys* 1984;**246**:H508-17.

26. Cabrales P, Tsai AG, Frangos JA, Intaglietta M. Role of endothelial nitric oxide in microvascular oxygen delivery and consumption. *Free Radic Biol Med* 2005;**39**:1229-37.

27. Intaglietta M, Tompkins WR. Microvascular measurements by video image shearing and splitting. *Microvasc Res* 1973;**5**:309-12.

28. Ortiz D, Cabrales P. Microhemodynamic parameters quantification from intravital microscopy videos. *Physiol Meas* 2014;**35**:351.

29. Lipowsky HH, Zweifach BW. Application of the "two-slit" photometric technique to the measurement of microvascular volumetric flow rates. *Microvasc Res* 1978;**15**:93-101.

30. Childs EW, Udobi KF, Wood JG, Hunter FA, Smalley DM, Cheung LY. *In vivo* visualization of reactive oxidants and leukocyte-endothelial adherence following hemorrhagic shock. *Shock* 2002;**18**:423-7.

31. Behrendt AK, Beythien M, Huber J, Zufrass T, Butschkau A, Mittlmeier T, et al. New TiAg composite coating for bone prosthesis engineering shows promising microvascular compatibility in the murine dorsal skinfold chamber model. *J Mater Sci Mater Med* 2015;**26**:5373.

32. Kraft CN, Burian B, Diedrich O, Gessmann J, Wimmer MA, Pennekamp PH. Microvascular response of striated muscle to common arthroplasty-alloys: A comparative in vivo study with CoCrMo, Ti-6Al-4 V, and Ti-6Al-7Nb. *J Biomed Mater Res A* 2005;**75**:31-40.

33. Kraft CN, Hansis M, Arens S, Menger MD, Vollmar B. Striated muscle microvascular response to silver implants: A comparative in vivo study with titanium and stainless steel. *J Biomed Mater Res* 2000;**49**:192-9.

34. Liu H, Webster TJ. Nanomedicine for implants: A review of studies and necessary experimental tools. *Biomaterials* 2007;**28**:354-69.